



**HAL**  
open science

## First SOLEDGE3X-EIRENE simulations of the ITER Neon seeded burning plasma boundary up to the first wall

S. Sureshkumar, N. Rivals, P. Tamain, X. Bonnin, R. Pitts, Y. Marandet, G. Ciruolo, H. Bufferand, G. Falchetto, N. Fedorczak, et al.

### ► To cite this version:

S. Sureshkumar, N. Rivals, P. Tamain, X. Bonnin, R. Pitts, et al.. First SOLEDGE3X-EIRENE simulations of the ITER Neon seeded burning plasma boundary up to the first wall. Nuclear Materials and Energy, 2024, 41, pp.101780. 10.1016/j.nme.2024.101780 . hal-04948159

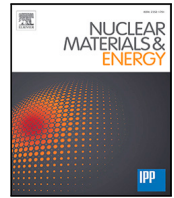
**HAL Id: hal-04948159**

**<https://hal.science/hal-04948159v1>**

Submitted on 14 Feb 2025

**HAL** is a multi-disciplinary open access archive for the deposit and dissemination of scientific research documents, whether they are published or not. The documents may come from teaching and research institutions in France or abroad, or from public or private research centers.

L'archive ouverte pluridisciplinaire **HAL**, est destinée au dépôt et à la diffusion de documents scientifiques de niveau recherche, publiés ou non, émanant des établissements d'enseignement et de recherche français ou étrangers, des laboratoires publics ou privés.



# First SOLEDGE3X-EIRENE simulations of the ITER Neon seeded burning plasma boundary up to the first wall

S. Sureshkumar<sup>a,\*</sup>, N. Rivals<sup>a</sup>, P. Tamain<sup>a</sup>, X. Bonnin<sup>b</sup>, R. Pitts<sup>b</sup>, Y. Marandet<sup>c</sup>, G. Ciraolo<sup>a</sup>, H. Bufferand<sup>a</sup>, G. Falchetto<sup>a</sup>, N. Fedorczak<sup>a</sup>, V. Quadri<sup>a</sup>, M. Raghunathan<sup>c</sup>, F. Schwander<sup>d</sup>, E. Serre<sup>d</sup>, R. Düll<sup>a</sup>, N. Varadarajan<sup>a</sup>

<sup>a</sup> CEA, IRFM, 13108 Saint-Paul-lez-Durance, France

<sup>b</sup> ITER Organisation, CS 90 046 - 13067 St Paul Lez Durance Cedex, France

<sup>c</sup> Aix-Marseille Université, CNRS, PIIM, Marseille, France

<sup>d</sup> Aix-Marseille Univ., CNRS, Centrale Méditerranée, M2P2, France

## ARTICLE INFO

### Keywords:

Edge plasma  
Simulation  
ITER  
Sputtering  
Plasma-neutral interaction

## ABSTRACT

Boundary plasma simulations are essential to estimate expected divertor and first wall (FW) heat and particle loads on ITER during burning plasma operation. A key missing feature of existing SOLPS simulations (Pitts et al., 2019) is the absence of a plasma solution out to the main chamber walls, essential to self-consistently estimate the gross sputtering of wall material. Here, SOLEDGE3X is applied for the first time to obtain up-to-the-wall burning plasma solutions of the ITER boundary plasma at the nominal  $P_{SOL} = 100$  MW of the main SOLPS database simulations, including He ash, Ne seeding but without fluid drifts. Compared with the most recent SOLPS-ITER simulations, our simulations show differences in the exact impurity distribution, but the key results for divertor and wall heat flux remain consistent. In the context of the ITER re-baselining exercise (Pitts, 2024), in which the Be FW armour is proposed to be exchanged for tungsten (W), estimates of W wall sources are key to the assessment of likely core contamination and hence impact on fusion gain. We compare the W gross erosion rates due to the different species excluding W self-sputtering. For the cases simulated spanning 0.27%–0.47% separatrix-averaged Ne concentration and  $7.5 \times 10^{22} \text{ s}^{-1}$  –  $1.95 \times 10^{23} \text{ s}^{-1}$  D fuelling,  $\text{Ne}^{8+}$  remains the largest contributor to the sputtering flux with the largest source being the outer divertor and baffle. The species-wise contribution to W sputtering changes with fuelling with sputtering due to lower Ne charge states being significant at low D fuelling. In general, the gross W sputtering source is found to decrease with increase in D fuelling and increase with increased Ne seeding.

## 1. Introduction

Modelling through numerical simulations of the plasma edge has been an essential part of the strategy for divertor design and for testing the operational space of current fusion devices [1,2]. A key component of such simulations is the interaction of the plasma with the neutral atoms present in the cooler regions of the chamber and the interaction of the plasma with the materials of the divertor and to a lesser extent the first wall. The results of such simulations are plasma solutions that give the density, temperature and other plasma parameters of each species in the plasma as well as fluxes of particles or energy to plasma-facing surfaces. Such a plasma solution can then be used by various codes to model different processes and scenarios, for example, erosion estimates using ERO 2.0.

For ITER such edge simulations were previously performed with multi-fluid modelling 2D axisymmetric in transport mode using the SOLPS-ITER code both for the low power scenarios (previously called Pre-Fusion Phase Operation or PFPO) [3] and the burning plasma scenarios (previously Fusion Power Operation or FPO) [4,5]. In parallel, a modelling program for these scenarios is underway using SOLEDGE3X-EIRENE [6] with the goal to confirm SOLPS results with another code and to obtain a plasma solution with a self-consistent far-SOL plasma solution - a key detail missing in existing SOLPS-ITER simulations. This detail is especially of importance in the presence of impurity seeding whose charge-state distribution in the far-SOL largely dominates the erosion on the first wall. Current studies [7] that use onion-skin models to extend SOLPS-ITER plasma solutions to the wall, find that the Ne impurity is responsible for a substantial fraction of the sputtered W wall

\* Corresponding author.

E-mail address: [srikanth.sureshkumar@cea.fr](mailto:srikanth.sureshkumar@cea.fr) (S. Sureshkumar).

<https://doi.org/10.1016/j.nme.2024.101780>

Received 5 July 2024; Received in revised form 11 October 2024; Accepted 16 October 2024

Available online 23 October 2024

2352-1791/© 2024 The Authors. Published by Elsevier Ltd. This is an open access article under the CC BY license (<http://creativecommons.org/licenses/by/4.0/>).

source. Verifying these results with a self-consistently solved up-to-the wall plasma solution is especially relevant in the context of the ITER rebaselining [8] where the ITER first wall is planned to be made of tungsten (W) instead of beryllium (Be).

Here we present the first results for the ITER edge plasma simulation with a self consistent far-SOL for the  $Q = 10$  burning plasma scenarios and analyse them in context of its impact on First wall (FW) erosion. In the following section (Section 2), the set up of SOLEDGE3X-EIRENE used to perform these ITER burning edge plasma simulations are discussed followed in Section 3 by the key results in terms of the response of the plasma to the fuelling and seeding, the mid-plane and target profiles compared to the SOLPS simulations for the same gas puffs, and the gross sputtering source of W from the wall. Finally Section 4 discusses these results on the in the context of the impact of impurity seeding and the main sputtering species.

## 2. Set-up for SOLEDGE3X-EIRENE simulations

SOLEDGE3X-EIRENE consists of a multi-fluid plasma solver SOLEDGE3X which is capable of simulating the edge plasma of fusion devices in 2D axisymmetric or 3D starting from inside the separatrix going up to the wall. It can be run in transport mode with user-specified assumptions on SOL transport perpendicular to the magnetic field, or in turbulence mode where the perpendicular transport is obtained self consistently. For modelling the plasma-wall interactions and plasma sources from neutrals, it is iteratively coupled to EIRENE - a Monte-Carlo solver for kinetic neutrals that takes the wall fluxes and plasma conditions from SOLEDGE3X as input. On every EIRENE call, the particle, momentum and energy sources from neutrals are computed considering the atomic reactions included in the 'Kotov model' [9] and passed to the plasma solver.

The simulation results for the ITER edge burning plasma shown in this paper were performed in 2D axisymmetric transport mode without fluid drifts. All simulations input parameters were set to the same values used for these scenarios in SOLPS simulations [4]. The plasma scenarios have  $Q_{plasma} = 10$  and a total power of  $P_{SOL} = 100$  MW is considered to enter the boundary plasma from the core. The core-edge boundary is considered to have a constant flux of He ash coming due to fusion in the core. Perpendicular transport coefficients are set to model an H-mode transport barrier, with diffusion coefficients for particles and heat respectively set to  $D_{\perp} = 0.03 \text{ m}^2 \text{ s}^{-1}$ ,  $\chi_{\perp} = 0.3 \text{ m}^2 \text{ s}^{-1}$  inside the transport barrier (poloidally uniform in closed flux-surfaces with a 4 cm width inside the separatrix at the outboard mid-plane), and set to  $D_{\perp} = 0.3 \text{ m}^2 \text{ s}^{-1}$  and  $\chi_{\perp} = 1 \text{ m}^2 \text{ s}^{-1}$  elsewhere. In order to keep the divertor targets under the engineering constraints in heat loads and electron temperature, the ITER burning plasma scenarios are partially detached and have Neon (Ne) as a seeded impurity injected as a gas puff to obtain this partial detachment.

For the purposes of modelling, the fuel is considered to be pure Deuterium (D) and the different cases discussed correspond to a different amount of D fuelling and Ne seeding rate. Both gases are puffed from the outer top fuelling port and the pump is considered to be under the dome shown by the green triangle and red surface respectively in Fig. 1. The power in the SOL was split equally between electrons and Deuterium at 50 MW each and a constant uniform He flux of  $1.0 \times 10^{20}$  ions/s at 1800 eV was assumed to enter the core-edge boundary as a fusion by-product. EIRENE is coupled to SOLEDGE3X through an interface STYX [10, section 2.4]. EIRENE called at every time step with a maximum CPU time of 10 s allocated for launching particles for each stratum. In practise this amounts to  $\sim 5000$  particles launched at every Eirene call. In previous work [10, Appendix D.2] for pure H scenarios this order of magnitude was found to be a good balance between performance and accuracy. The walls of the machine excluding the pumping surface were assumed to be perfectly reflecting with a particle recycling coefficient  $R = 1$  and the pumping surface is considered to have a 0.72% chance of pumping out an incident particle ( $R =$

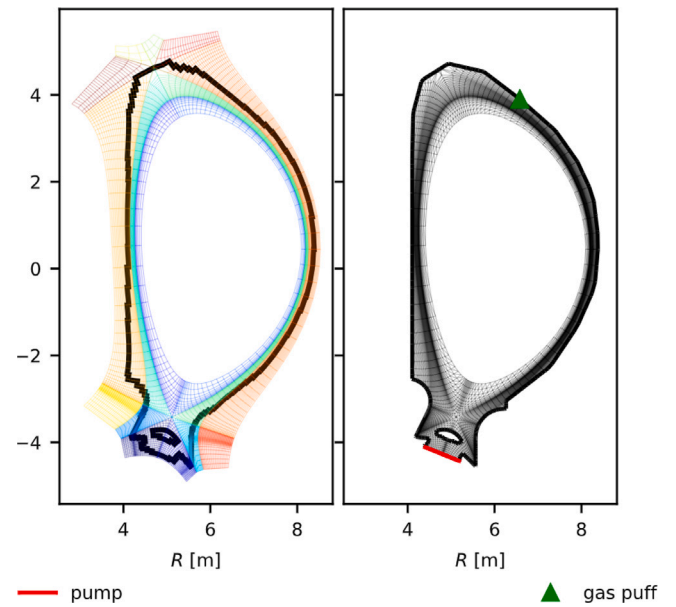


Fig. 1. SOLEDGE3X (left) and EIRENE (right) mesh used in the ITER burning plasma simulations. The gas puff location (green triangle) and pumping location (red surface) are marked on the EIRENE mesh. (For interpretation of the references to colour in this figure legend, the reader is referred to the web version of this article.)

Table 1  
Database of SOLEDGE3X-EIRENE simulations by input fuelling and seeding.

Shot no	D puff rate [ $\text{s}^{-1}$ ]	Ne puff rate [ $\text{s}^{-1}$ ]
123 008	7.50E+22	5.50E+19
123 009	1.00E+23	4.00E+19
123 010	1.95E+23	5.00E+19
123 011	1.95E+23	1.00E+20
123 012	1.95E+23	1.10E+20
123 013	1.95E+23	2.00E+20

0.9928). Finally, the walls and divertor are both assumed to be made of Beryllium (Be) following the assumptions on Be coating made in previous simulations of the ITER edge plasma [2]. Similar simulations but with a full W wall are currently running and will be investigated for future publication, but preliminary results suggest little impact on the results presented here in partially detached plasma conditions.

These simulations are continued until the plasma reaches steady state and is considered converged with respect to particle and energy balance following the criteria in [11] with the condition on the difference in particle influx and outflux being 5% instead of 1% due to the long convergence times of these simulations and the relative steadiness in plasma conditions. In order to reduce the total computation time, an acceleration scheme as described in [12] was implemented in SOLEDGE3X and used to reach steady state at an earlier plasma time in the simulations. The database of 6 burning plasma simulations was built corresponding to shot numbers 123 008–123 013 from the ITER IMAS database. The database covers a scan of throughput for the D fuelling at similar Ne seeding (123 008–123 010) as well as different Ne seeding at constant D fuelling (123 010–123 013) as shown in Table 1.

## 3. Results

The SOLEDGE3X simulations performed here are the first plasma edge plasma solutions with a self consistent far-SOL for the ITER burning plasma. These plasma solutions are first compared to the existing SOLPS-ITER simulations [4] for these cases in terms of the response of divertor neutral pressure, plasma quantities at the mid-plane and divertor targets. The plasma solutions obtained here are expected to

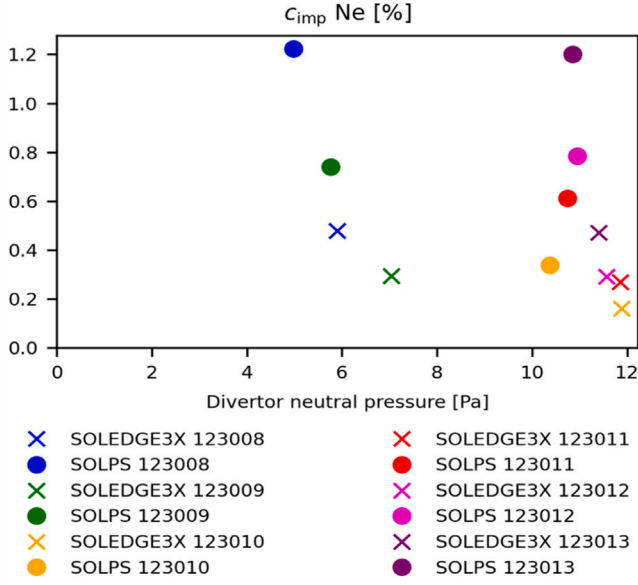


Fig. 2. Separatrix averaged impurity concentration vs. divertor neutral pressure for SOLEDGE3X (cross) and SOLPS (dots) simulations.

have some differences from that obtained from SOLPS due to the two codes having slight differences in the model (for example the inclusion of parallel currents in SOLPS which are not solved in SOLEDGE3X), differences in numerical scheme (e.g., a five point stencil in SOLPS vs. a nine point stencil in SOLEDGE3X) and of course differences in domain extension. Hence, this comparison should not be considered to be a benchmark but as a check to see if the codes produce qualitatively the same plasma conditions under the same inputs.

The first-wall conditions are investigated and used to obtain an estimate for the gross sputtering due to impurities as well as identify the most significant sources of W sputtering in terms of machine region and sputtering species.

### 3.1. Divertor neutral pressure and impurity concentration

An important quantity that characterises divertor performance is the divertor neutral pressure  $P_{\text{neutr}}$  [2] which is defined as the average of the total pressure due to atoms and molecules at the cells going from the dome along the private flux region boundary up to a short distance before the outer target. The cells are chosen to be consistent with the region used for neutral pressure calculation in SOLPS. It characterises the ability of the divertor to build up the neutral pressure to promote pumping and particle exhaust. The response of the plasma to the seeding of impurities is characterised by the separatrix averaged impurity concentration  $c_{\text{imp}}$  defined for an impurity of atomic number  $Z$  in terms of the electron density  $n_e$  as:

$$c_{\text{imp}} = \sum_{i=1}^Z \frac{n_i}{n_e} \quad (1)$$

The response of the neutral pressure in these SOLEDGE3X simulations were found to differ significantly from existing SOLPS simulations. Fig. 2 shows the position of these simulations in the  $(P_{\text{neutr}}, c_{\text{imp}})$  plane. It is seen that SOLEDGE3X simulations show consistently lower impurity concentration for the same fuelling and seeding puffs. Similarly the neutral pressure for corresponding cases are always higher in SOLEDGE3X with cases having the same D fuelling (123 010–123 013) having nearly the same divertor neutral pressure of  $\approx 11.8$  Pa. These differences mean that the plasma solution obtained by SOLEDGE3X and SOLPS differ under the same throughput conditions.

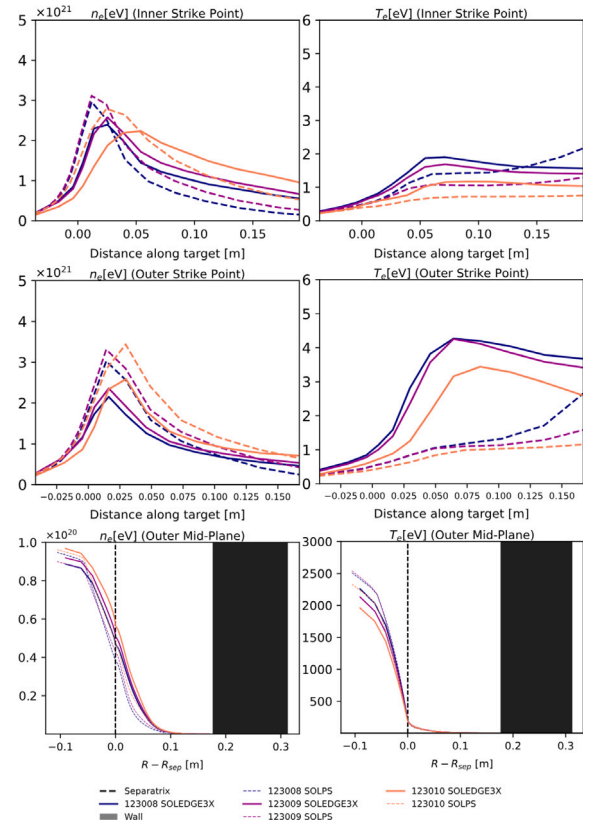


Fig. 3. Inner, outer target (first two rows) and mid-plane (final row) profiles of  $n_e$  (left) and  $T_e$  (right) in SOLEDGE3X and SOLPS simulations.

### 3.2. Midplane and target profiles

To compare the general response of the plasma to fuelling, the target and mid-plane profiles of electron density  $n_e$  and temperature  $T_e$  are compared for cases with different D and Ne injection in Fig. 3.

The target profiles for the cases of the D fuelling scan show that in SOLEDGE3X, the peak electron temperature increases with decrease in fuelling with the effect being more pronounced at the outer target compared to the inner target.  $T_e$  profiles in SOLEDGE3X show significant asymmetry between inner and outer targets and are in general more peaked than the flat profiles found in SOLPS. The target  $n_e$  profiles have a similar shape on both targets but are slightly more spread in SOLEDGE3X compared to SOLPS.

The midplane profiles in SOLEDGE3X for  $n_e$  and  $T_e$  are similar in shape to SOLPS. In SOLEDGE3X the  $n_e$  are larger for larger fuelling while the behaviour is opposite in SOLPS. The profiles for  $T_e$  differ significantly inside the separatrix between SOLEDGE3X and SOLPS with the former having an inverse relationship between the values of  $T_e$  and the fuelling amount while  $T_e$  is almost insensitive to the fuelling in SOLPS-ITER.

Overall, SOLEDGE3X predicts qualitatively similar plasma conditions to SOLPS. An investigation into the differences, their impact on the plasma solution, as well as similar differences observed also in pure H, low power (PFPO) ITER simulations (N. Rivals, et al.; NF 2024 submitted) is ongoing.

### 3.3. First wall and dome conditions

An important result obtained from the SOLEDGE3X simulations are the first wall conditions in terms of particle and energy fluxes to the wall. The extraction of these quantities are possible self-consistently

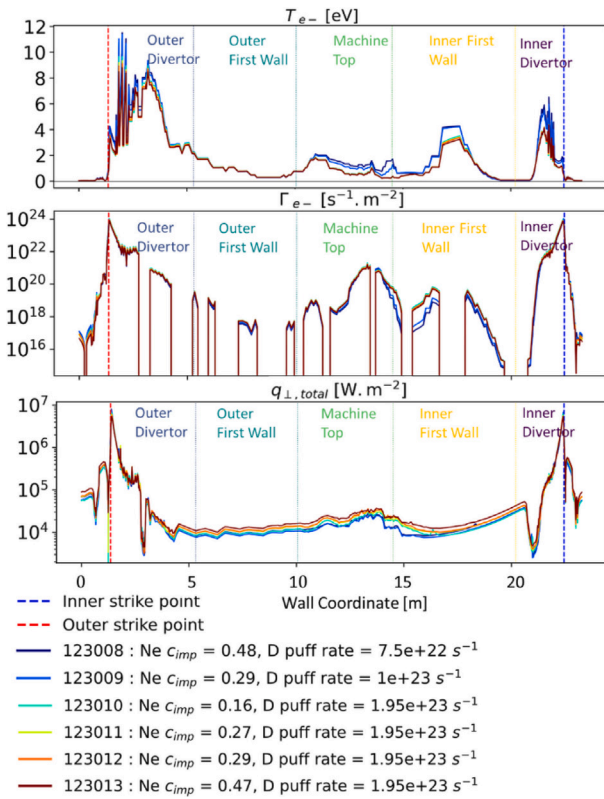


Fig. 4. Electron temperature  $T_e$ , Electron Flux  $\Gamma_e$ , and total heat flux  $q_{\perp,\text{total}}$  along the wall. Note the logarithmic scale.

without any further assumptions regarding the far-SOL in SOLEDGE3X since the simulation domain goes up to the wall. The electron temperature  $T_e$ , electron particle flux  $\Gamma_e$  and total perpendicular heat flux including radiation  $q_{\perp,\text{total}}$  are plotted along the wall in Fig. 4. These quantities are plotted starting from the outer strike point, going along the outer wall, the top of the machine, the inner wall, and inner strike point. The wall regions are labelled with the outer divertor region also including the outer baffle.

The electron temperature  $T_e$  is found to be large only around the divertor regions while most of the first wall has  $T_e < 2$  eV across the whole database except at the inner mid-plane where  $T_e$  goes up to 4 eV. It is influenced by fuelling with larger values of  $T_e$  seen at the top of the machine for cases with lower fuelling. The electron flux at the first wall is almost constant across the database with differences only seen at the top of the machine where the electron flux is lower at lower fuelling. The heat flux around the wall is of particular interest since it shows how effectively the Ne spreads the heat from the confined regions of the plasma to the rest of the wall. The first wall fluxes show that as the Ne seeding increases, the outer first wall heat flux increases by around 10 kW. This is accompanied by a reduction in the target heat fluxes where the peak heat flux is reduced by 200 kW as the Ne concentration is increased from  $c_{\text{imp}} = 0.16\%$  to  $c_{\text{imp}} = 0.47\%$ . From Table 2 which tabulates the integrated heat load on the walls for these cases, it can be seen that the percentage of the total heat load on the first wall increases from 7.24% to 9.8% following this increase in Ne concentration. An important caveat regarding the interpretation of the first wall heat flux in these simulations is that these simulation assume an axisymmetric wall and do not account for any shaping or impact of the segmented geometry of the actual wall.

The total integrated heat incident on the wall and the dome is tabulated in Table 2. There is a significant fraction of the heat flux of  $\sim 4\text{--}5\%$  on the dome however, this heat flux is limited to the top surface

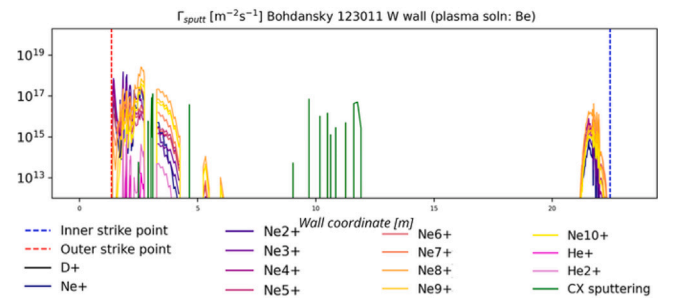


Fig. 5. Gross sputtered flux [ $\text{m}^{-2} \text{s}^{-1}$ ] of W for #123011 around the first wall split by sputtering ion species. Note the logarithmic scale.

of the dome which will be in W. The dome has a nearly zero incident flux of electrons across its surface except at the upper corners which experiences a peak localised electron flux of  $\Gamma_e = 10^{21} \text{ s}^{-1}$ . However, the electron temperature remains below 1 eV along the dome in all scenarios leading to no sputtering contribution from the dome.

### 3.4. Total radiated power by Ne

An important quantity of interest with regard to the impact of Ne seeding on plasma performance is the radiated power by the impurity. In the scenarios modelled here the power radiated in the edge by Ne increases with separatrix averaged Ne concentration increasing from  $\sim 13\%$  to  $\sim 29\%$  of the total input power as  $c_{\text{imp}}$  goes from 0.16% to 0.47% (Table 2). Among the Ne species, the most dominant radiating species is  $\text{Ne}^{5+}$  in all scenarios except 123 009 where it is  $\text{Ne}^{7+}$ .

### 3.5. Gross sputtering flux in #123011

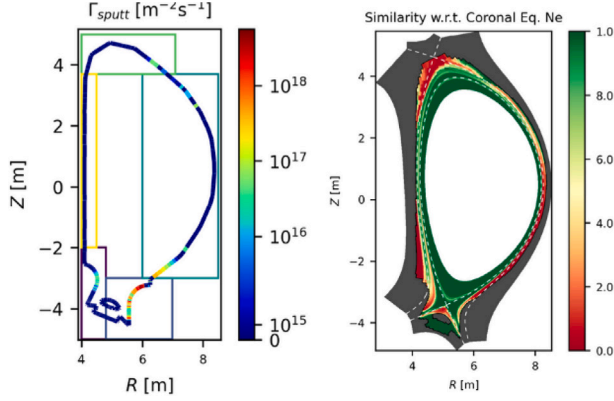
An important change in the newly proposed baseline for ITER is the change of first wall material to W from Be. The SOLEDGE3X simulations here are performed assuming a Be wall. Under the assumption that the wall material has little impact on the plasma background [5], we can nevertheless use these simulations to estimate the W gross erosion yields and the sputtered W source using the Bohdansky–García-Rosales formula [13] using the fit parameters for W wall. This gross sputtering yield was calculated by considering a shifted Maxwellian velocity distribution for all the ion species simulated in the plasma. However, since W was not evolved in these plasma simulations, no self sputtering contribution or re-deposition was included in this analysis. Additionally the sputtering due to atoms was obtained from EIRENE and is considered to be due to charge exchange.

Fig. 5 shows the incoming sputtered flux of tungsten from around the first wall decomposed by sputtering species for the case #123011. It can be seen that most of the sputtered flux of W comes from the outer divertor with a minor source at the top of the machine and the inner divertor. The largest contributing source of W sputtering were the highly ionised states of Ne in particular  $\text{Ne}^{8+}$ . A notable exception is the immediate vicinity of the outer strike point, where  $\text{Ne}^{2+}$  and  $\text{Ne}^{3+}$  dominate. The only sputtering source at the top of the machine is due to charge exchange from neutrals. This is explained by its proximity to the gas puff location.

The total W sputtered flux is shown on the left side of Fig. 6. The wall regions were divided into separate regions as shown by the boxes and integrated for analysis. The largest W source can be clearly identified as the outer baffle and the lower outer wall. The small charge exchange sputtering source can be seen near the gas injection part at the outer top of the machine and the only other significant W source is the inner divertor.

**Table 2**  
Integrated heat load on different plasma facing components and power radiated by different elements  $P_{elt}^{rad}$ .

Shot	Outer Div. $q_{\perp,tot}$ [W]	Wall $q_{\perp,tot}$ [W]	Inner Div. $q_{\perp,tot}$ [W]	Dome $q_{\perp,tot}$ [W]	(%) wall	(%) dome	$P_{Ne}^{rad}$ [W]	$P_D^{rad}$ [W]	$P_{He}^{rad}$ [W]
123 008	5.49E+07	7.05E+06	3.29E+07	4.62E+06	7.09%	4.65%	2.42E+07	1.46E+07	9.26E+05
123 009	5.50E+07	6.47E+06	3.35E+07	4.29E+06	6.52%	4.32%	1.80E+07	1.70E+07	8.57E+05
123 010	5.33E+07	7.17E+06	3.42E+07	4.44E+06	7.24%	4.48%	1.28E+07	2.35E+07	6.04E+05
123 011	5.24E+07	8.23E+06	3.35E+07	5.04E+06	8.30%	5.08%	1.99E+07	2.23E+07	5.39E+05
123 012	5.14E+07	8.53E+06	3.33E+07	5.07E+06	8.67%	5.15%	2.08E+07	2.22E+07	5.36E+05
123 013	5.09E+07	9.76E+06	3.31E+07	5.76E+06	9.80%	5.79%	2.90E+07	2.11E+07	4.89E+05



**Fig. 6.** Total W sputtered flux due to all sources (left) with the wall regions integrated over marked with boxes. Similarity index  $\Delta_{CE}$  (right) of Ne charge state distribution with that from coronal equilibrium as defined in Eq. (5). (For interpretation of the references to colour in this figure legend, the reader is referred to the web version of this article.)

### 3.6. Gross sputtering by machine region and species

To obtain general trends on first wall erosion under different fuelling and seeding conditions, the erosion analysis was performed for all the ITER burning plasma simulations in the SOLEDGE3X database. The sputtered flux of W was integrated for each case for different wall regions and sputtering species (Fig. 7).

The regions were broken down as shown by the boxes in the left side in Fig. 6. The integrated sputtered source shows that the total sputtering decreases with more fuelling and increases with higher Ne seeding.

In all the simulations, the largest W sputtering occurs on the outer divertor and baffle. A smaller but significant source is the outer first wall (mainly at the bottom just above the divertor and at the top close to the vertical port) whose contribution decreased on an increase of D fuelling. At very low fuelling (123 008) a small W source can also be seen at the inner divertor. When the sputtered W source is broken down by sputtering species, it is seen that it is dominated by  $Ne^{8+}$  which consistently accounts for more than 40% of the total W source. The percentage of W due to the highly ionised charge states remains consistent across the database of simulations but at lower fuelling (123 008 and 123 009) the sputtering due to  $Ne^{1+}$  -  $Ne^{4+}$  become significant. The charge exchange sputtering source remains small across the whole database and shows no clear trend on increasing fuelling and seeding.

## 4. Discussion and conclusion

Ne seeding in ITER burning plasma is found to reduce the target heat fluxes by spreading it along the first wall (Fig. 4). This effect increases with increasing Ne seeding suggesting that from the point of view of divertor heat load management, it is beneficial to run with a larger Ne seeding.

On the other hand, increasing the Ne seeding increases the total sputtered W source. The total erosion source depends on both the flux

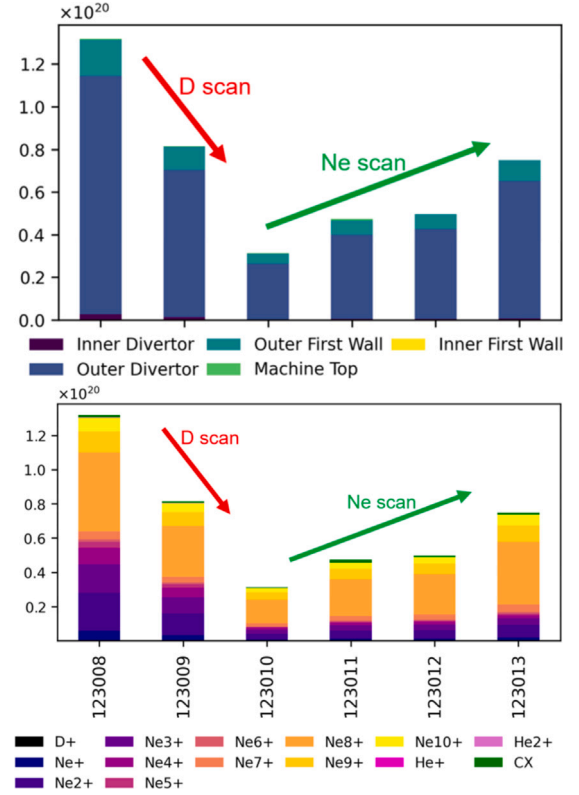


**Fig. 7.** Integrated W source (part/s) by first wall region (top) and by sputtering species (bottom) for different fuelling and Ne seeding scenarios.

of incident ions and the electron temperature  $T_e$ . However, since the electron temperature does not change appreciably on increasing the Ne seeding Fig. 4, it is the increased flux of high Z Ne ions at the first wall which is responsible for the increase in the sputtered W source. The dominance of the sputtering from large Z Ne states, in particular  $Ne^{8+}$ , indicates a large particle flux of high Z ions to the wall across the database which seems contradictory with the low electron temperature conditions encountered in the far SOL, unless the plasma is far from coronal equilibrium in that region.

The plasma reaches coronal equilibrium when the population of all charge states ( $n_z$ ) reaches equilibrium with respect to ionisation and recombination. If the ionisation rate and recombination rate are respectively  $S_z$  and  $\alpha_z$  for the charge state  $z$ , the evolution of density of the state  $n_z$  is given in terms of the electron density  $n_e$  and the rates as:

$$\frac{dn}{dt} = n_e n_{z-1} S_{z-1} - n_e n_z S_z + n_e n_{z+1} \alpha_{z+1} - n_e n_z \alpha_z \quad (2)$$

At steady state, for a total of  $N$  atoms, this leads to the analytical solution for coronal equilibrium density as:

$$n_z = \Pi_{i=0}^z \frac{S_i}{\alpha_{i+1}} n_0 \quad (3)$$

where the population of neutrals  $n_0$  is given by:

$$n_0 = \frac{N}{1 + \sum_{z=1}^Z \prod_{i=0}^z \frac{S_i}{\alpha_{i+1}}} \quad (4)$$

To investigate the deviation of the charge state distribution from coronal equilibrium for the case 123011, a cross correlation function was used defined by:

$$\Delta_{CE} = \frac{\sum_i n_{\text{real}}^{\text{Ne}^{i+}} n_{CE}^{\text{Ne}^{i+}}}{\sqrt{\sum_i n_{CE}^{\text{Ne}^{i+2}}} \sqrt{\sum_i n_{\text{real}}^{\text{Ne}^{i+2}}}} \quad (5)$$

Here,  $n_{\text{real}}^{\text{Ne}^{i+}}$  is the density of Neon species  $\text{Ne}^{i+}$  in the simulation and  $n_{CE}^{\text{Ne}^{i+}}$  is its density predicted from assuming coronal equilibrium. This is plotted on the right side of Fig. 6. Here, a value of  $\Delta_{CE} = 1$  (more green) means that locally the Ne is exactly in coronal equilibrium while a value closer to zero (more red) means it is far from it. It can be seen from the total sputtering in the same figure that in the regions where the total W source is large - close to the outer divertor and baffle, the plasma is far from coronal equilibrium. This is true in general in the colder parts of the plasma. In the vicinity of the outer baffle, Ne is more ionised with respect to coronal equilibrium with an average charge state of  $Z_{\text{avg}}^{\text{Ne}} = 5.27$  compared to the average charge state of  $Z_{\text{avg}}^{\text{Ne}}(\text{CE}) = 2.61$  predicted from coronal equilibrium. This is likely due to the time scale of transport to the wall being much smaller than the recombination time scale leading to an abundance of high Z charge states to the wall. The far SOL transport assumptions in these simulations assume a small and constant diffusion coefficient for the radial transport ( $D_{\perp} = 0.3 \text{ m}^2 \text{ s}^{-1}$ ,  $\chi_{\perp} = 1 \text{ m}^2 \text{ s}^{-1}$ ) and the sensitivity of these assumptions is to be tested particularly in the context of formation of density shoulders due to ballooning in the low field side as was done for the ITER low power operation phase in [14].

The charge state distribution of the sputtered species also reveals that low Z Ne states become significant at low fuelling. This is possibly due to the fact that peak of the incident energy distribution function for  $\text{Ne}^{4+}$  is very close to the threshold energy for W sputtering and therefore at high enough Ne fluxes the fraction of low Z Ne with energy over the sputtering threshold becomes significant.

The database of SOLEDGE3X-EIRENE simulations performed here cover a relatively small range of Ne separatrix concentration (Fig. 2) from 0.16% to 0.48%. Within this range, the Ne charge states that contribute most to W sputtering do not change. The range of Ne concentrations for which this continues to hold is to be investigated. Another factor that needs investigation is the impact of fluid drifts in these simulations and their impact on the large asymmetry between the W source from the inner and outer divertor. These could also be helpful in diagnosing the differences in plasma response to throughput seen with respect to SOLPS-ITER simulations. Finally, the plasma solutions obtained here assume that the wall and divertor are made of Be for the purposes of recycling. The exact impact of this assumption on the final plasma solution is to be investigated in further studies although initial investigation seem to indicate only a minor impact of the wall material on the plasma solution in such high recycling conditions.

The key consequence of the sputtered W source is the degradation of plasma performance the estimation of which requires W ions to be evolved in the fluid solver [15]. The sputtering source of W presented here only provide first estimates of the erosion characteristics of these scenarios. One needs kinetic codes such as ERO2.0 [16], in which such simulations can be used as background plasmas, to get a more quantitative estimate of net erosion and W migration. The availability of these up-to-the wall plasma backgrounds can form the basis for future W migration studies and wall shaping studies.

#### CRediT authorship contribution statement

**S. Sureshkumar:** Writing – review & editing, Writing – original draft, Validation, Software, Methodology, Investigation, Formal analysis, Data curation. **N. Rivals:** Writing – review & editing, Visualization,

Validation, Software, Methodology, Formal analysis, Data curation, Conceptualization. **P. Tamain:** Writing – review & editing, Validation, Supervision, Software, Resources, Project administration, Methodology, Investigation, Funding acquisition, Formal analysis, Conceptualization. **X. Bonnin:** Writing – review & editing, Supervision, Resources, Project administration, Funding acquisition. **R. Pitts:** Writing – review & editing, Validation, Supervision, Resources, Project administration, Funding acquisition. **Y. Marandet:** Writing – review & editing, Validation, Supervision, Resources, Project administration. **G. Ciraolo:** Writing – review & editing, Supervision, Resources, Project administration, Funding acquisition. **H. Bufferand:** Writing – review & editing, Software, Resources. **G. Falchetto:** Writing – review & editing, Project administration. **N. Fedorczak:** Writing – review & editing, Project administration. **V. Quadri:** Writing – review & editing, Software. **M. Raghunathan:** Software. **F. Schwander:** Software. **E. Serre:** Software. **R. Düll:** Software. **N. Varadarajan:** Software, Investigation.

#### Declaration of competing interest

The authors declare that they have no known competing financial interests or personal relationships that could have appeared to influence the work reported in this paper.

#### Acknowledgements

The views and opinions expressed herein do not necessarily reflect those of the ITER Organization. The authors thank the reviewers for their guidance in improving the manuscript. This work was performed under the auspices of the ITER Science Fellow Network and funded in part by contract IO/23/CT/4300002972. This work has been carried out within the framework of the EUROfusion Consortium, funded by the European Union via the Euratom Research and Training Programme (Grant Agreement No 101052200 — EUROfusion). Views and opinions expressed are however those of the author(s) only and do not necessarily reflect those of the European Union or the European Commission. Neither the European Union nor the European Commission can be held responsible for them.

#### Data availability

Data will be made available on request.

#### References

- [1] A. Kukushkin, H. Pacher, V. Kotov, G. Pacher, D. Reiter, Finalizing the ITER divertor design: The key role of SOLPS modeling, Fusion Eng. Des. 86 (12) (2011) 2865–2873, <http://dx.doi.org/10.1016/j.fusengdes.2011.06.009>, URL <https://www.sciencedirect.com/science/article/pii/S092037961100514X>.
- [2] R.A. Pitts, X. Bonnin, F. Escourbiac, H. Frerichs, J.P. Gunn, T. Hirai, A.S. Kukushkin, E. Kaveeva, M.A. Miller, D. Moulton, V. Rozhansky, I. Senichenkov, E. Sytova, O. Schmitz, P. Stangeby, G.D. Temmerman, I. Veselova, S. Wiesen, Physics basis for the first ITER tungsten divertor, Nucl. Mater. Energy 20 (2019) 100696, <http://dx.doi.org/10.1016/j.nme.2019.100696>, URL <https://www.sciencedirect.com/science/article/pii/S2352179119300237>.
- [3] J.-S. Park, X. Bonnin, R. Pitts, Assessment of ITER divertor performance during early operation phases, Nucl. Fusion 61 (1) (2020) 016021, <http://dx.doi.org/10.1088/1741-4326/ab73c1>.
- [4] E. Kaveeva, V. Rozhansky, I. Senichenkov, E. Sytova, I. Veselova, S. Voskoboinikov, X. Bonnin, R. Pitts, A. Kukushkin, S. Wiesen, D. Coster, SOLPS-ITER modelling of ITER edge plasma with drifts and currents, Nucl. Fusion 60 (4) (2020) 046019, <http://dx.doi.org/10.1088/1741-4326/ab73c1>.
- [5] J.-S. Park, X. Bonnin, R. Pitts, J. Lore, Impact of gas injection location and divertor surface material on ITER fusion power operation phase divertor performance assessed with SOLPS-ITER, Nucl. Fusion 64 (3) (2024) 036002, <http://dx.doi.org/10.1088/1741-4326/ad1d11>.
- [6] N. Rivals, P. Tamain, Y. Marandet, X. Bonnin, H. Bufferand, R.A. Pitts, G. Falchetto, H. Yang, G. Ciraolo, SOLEDGE3X full vessel plasma simulations for computation of ITER first-wall fluxes, Contrib. Plasma Phys. 62 (5–6) (2022) e202100182, <http://dx.doi.org/10.1002/ctpp.202100182>, URL <https://onlinelibrary.wiley.com/doi/abs/10.1002/ctpp.202100182>.

- [7] K. Schmid, Full W ITER: assessment of expected wall erosion and implications of boronization on fuel retention, in: *Plasma Surface Interaction 26*, Marseille, 2024.
- [8] R.A. Pitts, Plasma-wall interaction impact of the ITER re-baseline, in: *Plasma Surface Interaction 26*, Marseille, 2024.
- [9] V. Kotov, D. Reiter, R.A. Pitts, S. Jachmich, A. Huber, D.P. Coster, J.-E. contributors, Numerical modelling of high density JET divertor plasma with the SOLPS4.2 (B2-EIRENE) code, *Plasma Phys. Control. Fusion* 50 (10) (2008) 105012, <http://dx.doi.org/10.1088/0741-3335/50/10/105012>.
- [10] N. Rivals, Understanding density regimes and divertor detachment in ITER relevant conditions (Ph.D. thesis), Aix-Marseille Université (AMU), 2023, URL <https://cea.hal.science/tel-04461920>.
- [11] S. Wiesen, D. Reiter, V. Kotov, M. Baelmans, W. Dekeyser, A. Kukushkin, S. Lisgo, R. Pitts, V. Rozhansky, G. Saibene, I. Veselova, S. Voskoboinikov, The new SOLPS-ITER code package, *J. Nucl. Mater.* 463 (2015) 480–484, <http://dx.doi.org/10.1016/j.jnucmat.2014.10.012>, URL <https://www.sciencedirect.com/science/article/pii/S0022311514006965>, *Plasma-Surface Interactions* 21.
- [12] E. Kaveeva, V. Rozhansky, I. Senichenkov, I. Veselova, S. Voskoboinikov, E. Sytova, X. Bonnin, D. Coster, Speed-up of SOLPS-ITER code for tokamak edge modeling, *Nucl. Fusion* 58 (12) (2018) 126018, <http://dx.doi.org/10.1088/1741-4326/aae162>.
- [13] C. García-Rosales, W. Eckstein, J. Roth, Revised formulae for sputtering data, *J. Nucl. Mater.* 218 (1) (1995) 8–17, [http://dx.doi.org/10.1016/0022-3115\(94\)00376-9](http://dx.doi.org/10.1016/0022-3115(94)00376-9), URL <https://www.sciencedirect.com/science/article/pii/0022311594003769>.
- [14] N. Rivals, P. Tamain, Y. Marandet, X. Bonnin, H. Bufferand, R.A. Pitts, G. Falchetto, H. Yang, G. Ciraolo, Impact of enhanced far-SOL transport on first wall fluxes in ITER from full vessel edge-plasma simulations, *Nucl. Mater. Energy* 33 (2022) 101293, <http://dx.doi.org/10.1016/j.nme.2022.101293>, URL <https://www.sciencedirect.com/science/article/pii/S2352179122001740>.
- [15] N. Varadarajan, Poster: SOLEDGE3x integrated core-edge modelling of tungsten sources, migration, and radiation in WEST plasmas, in: *Plasma Surface Interaction 26*, Marseille, 2024.
- [16] J. Romazanov, et al., ERO2. 0, a code for three-dimensional modelling of global material erosion, transport and deposition in fusion devices 28th IAEA fusion energy conf, 2021, Virtual Event.